NOLTA, IEICE

Paper

Homoclinic bifurcation analysis for logistic map

Yuu Miino [1 a)] *and Tetsushi Ueta* [2]

[1] *Dept. of Electric and Electronic Engineering, School of Engineering, Tokyo University of Technology,*
1404-1 Katakuramachi, Hachioji, Tokyo 192-0982, Japan

[2] *Center for Admin. Info. Tech., Tokushima University,*
2-1 Minamijosanjimacho, Tokushima, 770-0814, Japan

[a)] *miinoy@stf.teu.ac.jp*

Received October 13, 2021; Revised December 15, 2021; Published April 1, 2022

Abstract: In this study, we have developed the method to obtain the homoclinic bifurcation parameter of an arbitrary targeted fixed point in the logistic map T_r. We have considered the geometrical structure of T_r around $x = 0.5$ and derived the core condition of the bifurcation occurrence. As the result of numerical experiment, we have calculated the exact bifurcation parameter of the fixed point of T_r^ℓ with $\ell \leq 256$. We have also discussed the Feigenbaum constants found in the bifurcation parameter and the fixed point coordinate sequences. This fact implies the local stability of the fixed point and global structure around it are in association via the constants.

Key Words: homoclinic bifurcation, logistic map, global bifurcation, Feigenbaum constants

1. Introduction

Logistic map is the legacy nonlinear map developed by May[1]. This map has a quite simple formula but shows pretty complex chaotic motion. Some researchers use the chaotic property to encrypt an image[2]; others do the random bit generation[3], and so on. From another standpoint, Smale[4] has studied a chaotic diffeomorphism and has discovered a potential reason for such chaotic motion is the appearance of transversal homoclinic points, which are the cross points of the unstable and stable manifold of a fixed point.

However, there are few pieces of research considering the homoclinic point and its bifurcation of the logistic map. We have imagined the homoclinic bifurcation analysis had been difficult because the map is not diffeomorphism (in this case, non-invertible). In this study, we discover the core condition of the homoclinic bifurcation occurrence and propose the numerical method to calculate the homoclinic bifurcation parameter.

This paper includes the following contents. In Sec. 2, we confirm the mathematical preliminaries such as the definition of the map, fixed point and its local stability, stable and unstable manifolds, and so on. The definition of the manifolds is specific to the non-invertible map and thus is the key to our proposing method. In Sec. 3, we investigate the condition of the homoclinic bifurcation from

Nonlinear Theory and Its Applications, IEICE, vol. 13, no. 2, pp. 209–214 DOI: 10.1587/nolta.13.209

the easier example case to the general case. After the discussion, we derive the formulations that the bifurcation parameter and the corresponding fixed point must satisfy. In Sec. 4, we conduct the numerical experiments to show the validity of our method. In Sec. 5, we conclude this research.

2. System description

Logistic map is the discrete map defined by

$$T_r : [0,1] \subset \mathbb{R} \to \left[0, \frac{r}{4}\right] \subset \mathbb{R}; \quad x \mapsto rx(1-x), \tag{1}$$

where $r \in [0,4] \subset \mathbb{R}$ is a parameter. Considering the discrete-time dynamical system $x_{n+1} = T_r(x_n)$ for $n \in \mathbb{N}_0$, x^* is a fixed point of T_r^ℓ if $T_r^\ell(x^*) = x^*$ and $T_r^k(x^*) \neq x^*$ for $0 < k < \ell$.

In the neighborhood of the fixed point x^* of T_r, we can measure the asymptotic stability of x^* by the derivative of T_r:

$$\frac{dT_r}{dx}(x^*) = r(1-2x^*). \tag{2}$$

Let us call this derivative the eigenvalue of x^*. Depending on the eigenvalue, we can classify the stability of x^* as follows: x^* is stable if $|dT_r/dx| < 1$, and it is unstable otherwise. Also, the sign of the eigenvalue determines the behavior near x^*. In other words, the trajectory converges to (or diverges from) x^* oscillatively if the sign of the eigenvalue is negative, and they do without oscillation otherwise. For the fixed point of T_r^ℓ, we can derive the eigenvalue by the chain-rule:

$$\frac{dT_r^\ell}{dx}(x^*) = \frac{dT_r}{dx}(x_{\ell-1})\frac{dT_r}{dx}(x_{\ell-2})\cdots\frac{dT_r}{dx}(x^*) = r^\ell \prod_{n=0}^{\ell-1}(1-2x_n), \tag{3}$$

where $x_n = T_r^n(x^*)$.

According to Mira[5], the set of points $P_n(x') = \{x \mid x' = T^n(x)\}$ is the set of rank-n preimages of x'. Assume x^* be an unstable fixed point, stable and unstable manifolds of x^* are the sets of points

$$W^{\mathrm{s}}(x^*) = \{x \mid x \in P_n(x^*), n \in \mathbb{N}, \text{ and } x \neq x^*\}, \tag{4}$$

$$W^{\mathrm{u}}(x^*) = \left\{x \mid x^* \in \lim_{n\to\infty} P_n(x), \text{ and } x \neq x^*\right\}, \tag{5}$$

respectively. The definition of W^{u} in here is not general but specific to the non-invertible map. Homoclinic point of x^* is the point in the set $W^{\mathrm{s}}(x^*) \cap W^{\mathrm{u}}(x^*)$, as shown in Fig. 1; homoclinic bifurcation is the phenomenon of appearance and disappearance of the homoclinic points.

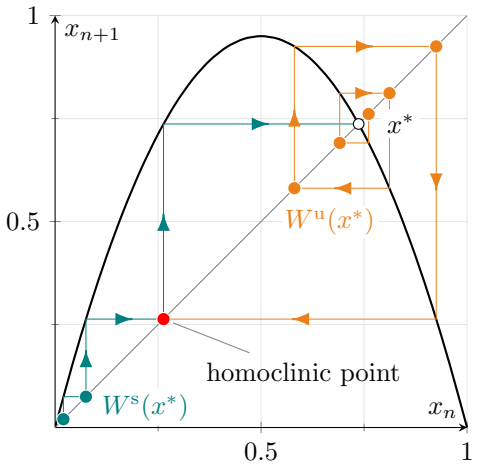

Fig. 1: Homoclinic point of a fixed point x^* of T_r.

3. Method of analysis

In this section, we derive the exact condition of the homoclinic bifurcations. Assume x^* is an unstable fixed point of T_r having a negative eigenvalue, i.e., $dT_r/dx < -1$.

As an easiest case to understand the condition, let us consider the case of $r = 3.6$ and discuss the schematic illustration in Fig. 2(a). In this figure, one of the rank-1 preimages locates at higher coordinate than $r/4$ (interval on upper right) and thus no further preimages available for this interval. On the other hand, the rest preimage locates entirely inside the source interval, i.e., the further preimages for this interval is recurrently inside itself. As the result, the rank-n preimages of the interval $[0, T_r^2(0.5))$ cannot contain the fixed point x^*. This implies the unstable manifold $W^{\mathrm{u}}(x^*)$ is the interval $[T_r^2(0.5), T_r(0.5)]$. The following two facts can explain the validity of this consideration. The first one is that the rank-n preimages of this interval are available for arbitrary higher value of n even if the preimages for $x > 0.5$ because they cannot go over $r/4$. The second is that preimages must asymptotically converge to x^* once they come into the local space of x^* because x^* is asymptotically unstable (trajectory with $W^{\mathrm{u}}(x^*)$ in Fig. 1 might help understanding this fact).

After the discussion of the unstable manifold $W^{\mathrm{u}}(x^*)$, it is easier to consider the stable manifold $W^{\mathrm{s}}(x^*)$. Figure 2(b) shows some points in $W^{\mathrm{s}}(x^*)$ with the backward-time trajectory. From the figure, we can confirm the rank-1 preimage is in the interval $[0, T_r^2(0.5)]$, so be the further preimages in $[0, T_r^2(0.5)]$ or $[T_r(0.5), 1]$. Therefore, from the above discussion, $W^{\mathrm{u}}(x^*) \cap W^{\mathrm{s}}(x^*) = \emptyset$ with $r = 3.6$. In addition, it is obvious that the most inside (nearest to $W^{\mathrm{u}}(x^*)$ in the sense of Euclid distance) points in $W^{\mathrm{s}}(x^*)$ are the rank-1 preimage and one in the rank-2 preimage (upper right one) because the preimages monotonically go away from x^*. This fact suggests that $W^{\mathrm{u}}(x^*) \cap W^{\mathrm{s}}(x^*)$ becomes not empty when it satisfies the following relations:

$$T_{r^*}(0.5) \in P_2(x^*) \quad \Leftrightarrow \quad T_{r^*}^2(0.5) \in P_1(x^*) \quad \Leftrightarrow \quad T_{r^*}^3(0.5) = x^*. \tag{6}$$

Figure 2(c) shows the situation of the homoclinic bifurcation with this equation.

In this example, we have focused on the case of $\ell = 1$ but the discussion is valid for the higher ℓ because the topological structure of T_r^ℓ around $x = 0.5$ is the same as T_r. Therefore, the homoclinic bifurcation parameter r^* and corresponding fixed point x^* of T_r^ℓ satisfies

$$T_{r^*}^\ell(x^*) - x^* = 0, \tag{7}$$

$$T_{r^*}^{3\ell}(0.5) - x^* = 0. \tag{8}$$

Equation (7) is the condition that x^* is the fixed point of T_r^ℓ; Eq. (8) is the condition generalized from Eq. (6) to be applicable to the map T_r^ℓ. We can simultaneously solve these conditions by numerical method such as Newton's method.

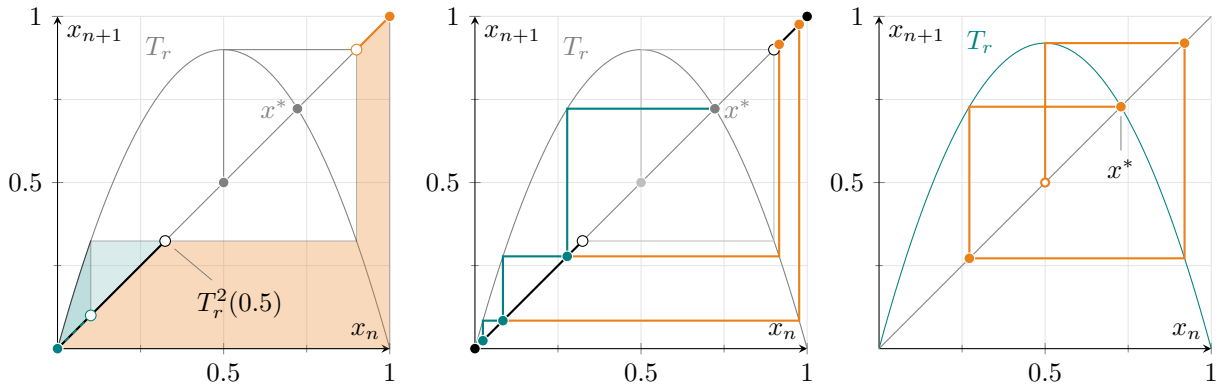

(a) Rank-1 preimages of the interval $[0, T_r^2(0.5))$.

(b) Stable manifold $W^{\mathrm{s}}(x^*)$.

(c) Situation of Eq. (6) with $r = 3.678\,573\ldots$

Fig. 2: Schematic illustrations of the proposing method with $r = 3.6$ and $r = r_1^*$.

4. Result of experiment

We have numerically derived (r_ℓ^*, x_ℓ^*) for $\ell = 2^k, k = 0, 1, \ldots 8$. We set the tolerance of condition Eqs. (7)–(8) in this experiment as 1×10^{-12}. Note that this tolerance is not the bottleneck of the proposing method. As mentioned around Tab. I, this tolerance should depend on the precision of the numeric number in the experiment.

Figure 3 shows the obtained bifurcation parameters with a one-parameter bifurcation diagram. We can see the parameters are always at the positions where the chaotic region separates into twice. This separation is a natural phenomenon because the homoclinic bifurcation affects the basin of the boundary. For example, with $r \in [r_2^*, r_1^*]$, the two fixed points of T^2 are under the homoclinic condition; this leads to the two chaotic motions with T^2 (which are symmetric to each other). However, they

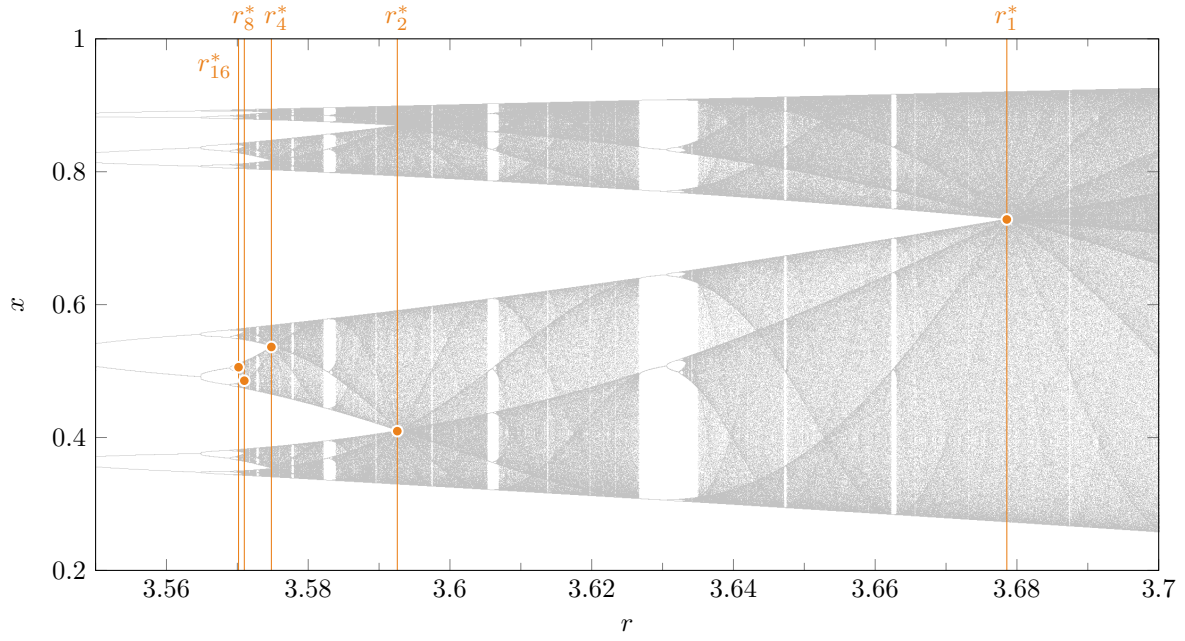

(a) $r \in [3.55, 3.7]$.

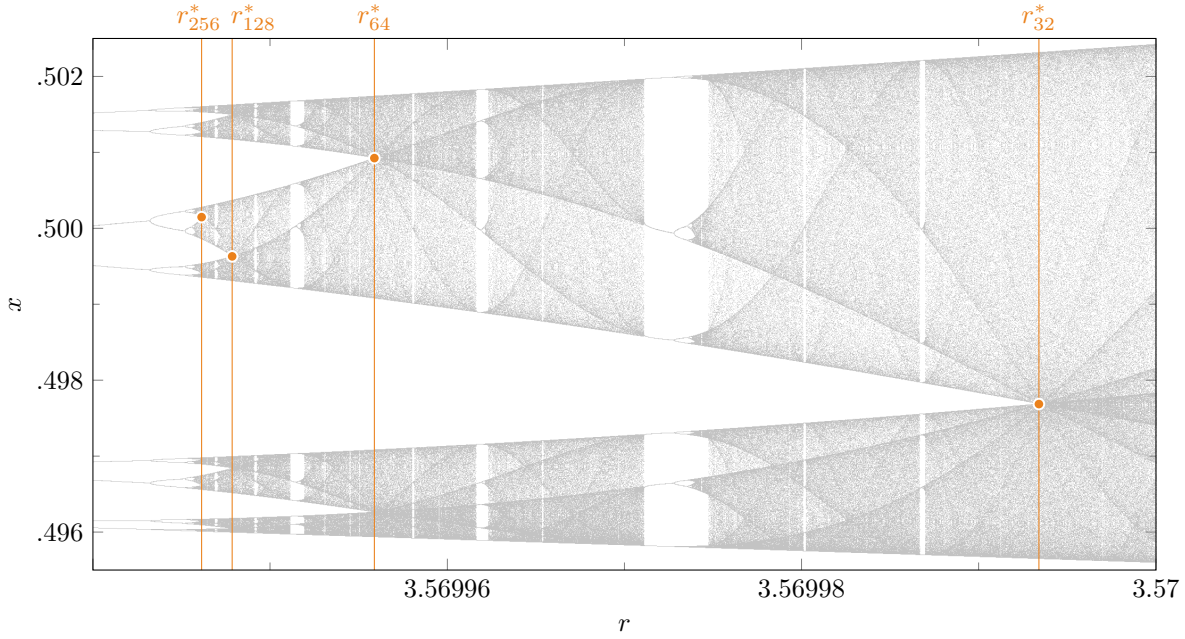

(b) $r \in [3.56994, 3.57]$.

Fig. 3: Experimental result in one-parameter bifurcation diagram. Vertical lines are the bifurcation parameters r_ℓ^* and outlined points on each line are the corresponding x_ℓ^*.

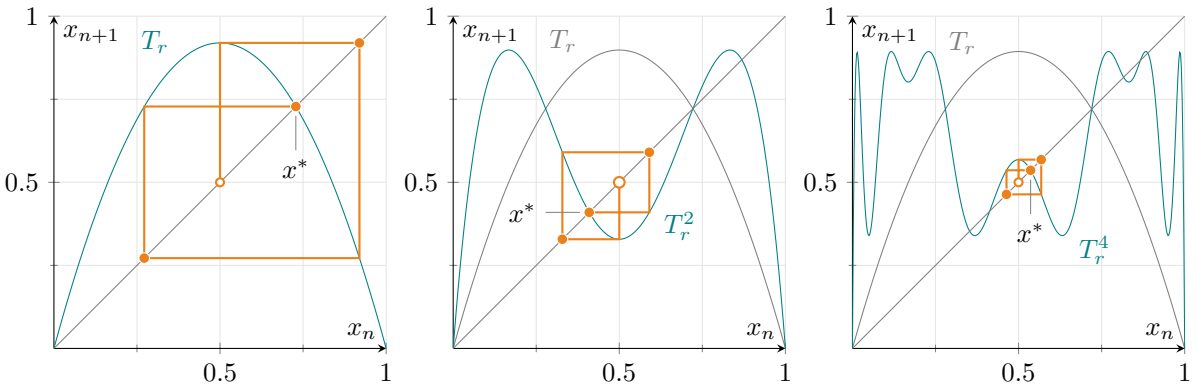

(a) $\ell = 1$. (b) $\ell = 2$. (c) $\ell = 4$.

Fig. 4: Return map at the homoclinic conditions with $\ell = 1, 2, 4$.

cannot go through the stable manifold of the fixed point of T because it is not in the homoclinic condition.

Figure 4 is the return maps at the homoclinic conditions. In these figures, we can find that x^* satisfies Eq. (7) and the corresponding trajectory does Eq. (8). Also, we can see the topological equivalence around $x = 0.5$ for each case.

The obtained bifurcation parameters are obviously equivalent to the band-splitting parameter[6] because the band-splitting is one of the side effects of the homoclinic bifurcation. This implies the homoclinic bifurcation also follows the Feigenbaum constants[7] as well as the period-doubling bifurcation. Let us confirm this fact with the following discussion. Feigenbaum constant δ is the limiting ratio defined by

$$\delta = \lim_{m\to\infty} \frac{a_{m-1} - a_{m-2}}{a_m - a_{m-1}} = 4.669\,201\,609\ldots, \tag{9}$$

where a_m is the m-th period doubling bifurcation parameter. We define a ratio δ_k defined by

$$\delta_k = \frac{r_{k-1} - r_{k-2}}{r_k - r_{k-1}}, \tag{10}$$

where $r_k = r_\ell^*$ with $\ell = 2^k$. Then, we find the value of δ_k converges to δ as k increases, as shown in Tab. I. Furthermore, we can see the second Feigenbaum constant $\alpha = 2.502\,907\,875\ldots$[8] in the sequence of the coordinates x_ℓ^*. Let d_k be the distance $d_k = x_k - 0.5$, and α_k be the ratio defined by

$$\alpha_k = \frac{d_k}{d_{k-1}}. \tag{11}$$

Then, we find the value of α_k converges to $-\alpha$ as k increases, as shown in Tab. I. This result implies that the homoclinic bifurcation strongly relates to the universal constants δ and α as well as the

Table I: Result of numerical values.

k	ℓ	r_ℓ^* (r_n)	x_ℓ^* (x_n)	error (2-norm)	δ_k	α_k
0	1	3.678 573 510 428	0.728 155 493 654	1.698×10^{-15}	-	-
1	2	3.592 572 184 107	0.409 580 677 437	6.327×10^{-14}	-	-
2	4	3.574 804 938 759	0.536 272 306 036	1.687×10^{-14}	4.840 442 321	−2.492 792 227
3	8	3.570 985 940 342	0.485 503 875 659	2.734×10^{-15}	4.652 331 163	−2.502 207 154
4	16	3.570 168 472 496	0.505 792 552 285	3.386×10^{-14}	4.671 741 446	−2.502 545 273
5	32	3.569 993 388 559	0.497 685 617 775	1.757×10^{-14}	4.669 005 392	−2.502 850 316
6	64	3.569 955 891 325	0.500 924 683 153	4.126×10^{-14}	4.669 249 390	−2.502 892 171
7	128	3.569 947 860 565	0.499 630 556 001	4.074×10^{-13}	4.669 201 171	−2.502 904 785
8	256	3.569 946 140 622	0.500 147 605 954	7.261×10^{-13}	4.669 201 246	−2.502 907 159

period-doubling bifurcation. In other words, local stability and global structure are in association via these constants.

Table I also summarizes the errors of Eqs. (7)–(8) in 2-norm of (r_ℓ^*, x_ℓ^*). In the cases of $k \leq 8$, the proposed method converges with the tolerance of 1×10^{-12}. On the other hand, the proposed method does not do well with this tolerance for $k > 8$. This is because the precision of the numeric numbers: x^*, r^*, or $T^n(x^*)$, is not enough for the huge counts of iterations. Therefore, the more k becomes the more precision this method requires to converge.

At last, this method is much sensitive to the initial condition of the numerical root-finding of Eqs. (7) and (8). The most general way that the author considers is seeing the one-parameter bifurcation diagram in detail. This takes much calculation or time costs but is highly reliable. On the other hand, one of the efficient way to get the proper initial condition is using the Feigenbaum constants to guess the condition of the next iteration. In this study, we have used the latter.

5. Conclusion

In this study, we have developed the method to obtain the homoclinic bifurcation parameter of an arbitrary fixed point. We have considered the geometrical structure of the logistic map around $x = 0.5$ and derived the core condition of the bifurcation occurrence. Focusing on the lower ℓ cases, we have conducted the numerical experiments and confirmed the validity of our method. As a result, we have calculated the exact bifurcation parameter of the fixed point of T_r^ℓ with $\ell \leq 256$. Even for the higher value of ℓ, we have expected that the precision improvement of numerical numbers will make our method go well. We have also discussed the Feigenbaum constants found in the bifurcation parameter and the fixed point coordinate sequences. This fact implies a possibility that the local stability and global structure around a fixed point are in the association via the Feigenbaum constants.

Our method described in this paper has focused on the periodic trajectory with oscillation, i.e., the case of $dT_r/dx < -1$. The authors consider the key to improving the method for the positive case is the count of iterations 3 in Eq. (8). Moreover, for generalization, we have to consider how we obtain the peak point of the map, e.g., the higher dimensional maps like multi-coupled systems. The authors should investigate the relationship between the proper peak point for our method and the root of the derivative zero. In future work, we would like to make discussion for these cases.

6. Acknowledgment

The authors give many thanks to Dr. Hiroshi Kawakami, who is the professor emeritus of Tokushima University, for his meaningful comments and discussions on this study.

References

[1] R. M. May, "Simple mathematical models with very complicated dynamics," *Nature*, vol. 261, p. 459, 1976.

[2] N. K. Pareek, V. Patidar, and K. K. Sud, "Image encryption using chaotic logistic map," *Image and vision computing*, vol. 24, no. 9, pp. 926–934, 2006.

[3] V. Patidar, K. K. Sud, and N. K. Pareek, "A pseudo random bit generator based on chaotic logistic map and its statistical testing," *Informatica*, vol. 33, no. 4, 2009.

[4] S. Smale, "Differentiable dynamical systems," *Bulletin of the American mathematical Society*, vol. 73, no. 6, pp. 747–817, 1967.

[5] C. Mira, *Chaotic dynamics in two-dimensional noninvertible maps*. World Scientific, 1996, vol. 20.

[6] H. Daido, "Universal relation of a band-splitting sequence to a preceding period-doubling one," Physics Letters A, vol. 86, no. 5, pp. 259–262, 1981.

[7] D. Jordan, P. Smith, and P. Smith, *Nonlinear ordinary differential equations: an introduction for scientists and engineers*. Oxford University Press on Demand, 2007, vol. 10.

[8] S. H. Strogatz, *Nonlinear dynamics and chaos with student solutions manual: With applications to physics, biology, chemistry, and engineering*. CRC press, 2018.